ELSEVIER

Journal of Structural Geology 26 (2004) 475–489

JOURNAL OF STRUCTURAL GEOLOGY

www.elsevier.com/locate/jsg

Problem of folding in ductile shear zones: a theoretical and experimental investigation

Nibir Mandal[a], Susanta Kumar Samanta[a], Chandan Chakraborty[b,*]

[a]*Department of Geological Sciences, Jadavpur University, Calcutta 700032, India*
[b]*Geological Studies Unit, Indian Statistical Institute, 203, B.T. Road, Calcutta 700035, India*

Received 3 December 2002; received in revised form 1 July 2003; accepted 1 July 2003

Abstract

The paper describes micro-scale folds within a narrow ductile shear zone of the Peninsular Gneissic Complex, South India. The characteristics of the folds indicate that they have formed by buckling on the mylonitic foliation parallel to the *C* fabric. This raises the question of how a buckling instability could develop on the mylonitic foliation, as there can be no overall shortening along the shear direction. On the basis of natural observations we show that mylonitization involves sericitization locally along the C fabrics, forming discrete mechanically weak zones, which perturb the homogeneous shear stress field in their neighborhood, and induce shortening along the bulk shear direction, leading to buckling instabilities on the mylonitic foliation. The weak zone model is supported with results obtained from physical experiments. Theoretical analysis shows that the weak bodies with large length-to-thickness ratios perturb the shear stress field in the shear zone significantly, developing compressive stresses along the bulk shear direction, required for buckle instabilities to occur on the mylonitic foliation.

Keywords: Mylonites; Weak sericite zone; Buckling; Foliation; Shear; Complex functions

1. Introduction

In spite of significant work on ductile shear zones over the last few decades, a fundamental question has remained virtually unresolved—how folds form on mylonitic foliations that are either parallel to the *XY*-plane of finite strain (*S*-fabric) or the shear zone boundary (*C*-fabric). Several models have been proposed to resolve this basic problem. According to Ramsay's (1980) model, initial geometrical irregularities can grow and accentuate with progressive shear, forming fold structures with strongly non-cylindrical shapes (Fig. 1a), as observed in physical experiments (Cobbold and Quinquis, 1980). Field observations, however, reveal that folds generally occur with a sinusoidal geometry with characteristic wavelengths, suggesting their development by buckling instabilities on the foliation (Ghosh and Sengupta, 1987; Fossen and Rykkelid, 1989; Mawer and Williams, 1991; Honge and Hippertt, 2001). Such buckling instability requires contraction along the foliation, which different workers have attempted to model in different ways. Passchier and Trouw (1996) have shown that discrete slip surfaces with a sidestepped arrangement can lead to local shortening along the foliation, giving rise to folds in the overlapping zone of the sidestepped shear surfaces (Fig. 1b). Ghosh and Sengupta (1987) pointed out that non-uniform slip along the foliation might result in shortening along the foliation, triggering buckle instability on the foliation. However, it has been demonstrated from kinematic considerations that development of folds under such a condition is mechanically difficult (Fig. 1c; Ez, 2000). There have also been attempts to show that folds can form locally due to curvilinear trajectories of the shear surfaces (Fig. 1d; Fossen and Rykkelid, 1989) or development of subsidiary shear surfaces at an angle to the mylonitic foliation (Fig. 1e; Ghosh and Sengupta, 1987; Harris, 2003). Bons and Urai (1996) have shown that folds can develop due to thickness variation in competent layers. Under layer-parallel shear the thicker portion of the layers rotate preferentially, giving rise to fold structures. Based on continuum models, some workers have demonstrated that fold structures can localize under the heterogeneous flow

* Corresponding author.
E-mail address: chandan@isical.ac.in (C. Chakraborty).

0191-8141/$ - see front matter © 2003 Elsevier Ltd. All rights reserved.
doi:10.1016/j.jsg.2003.07.004

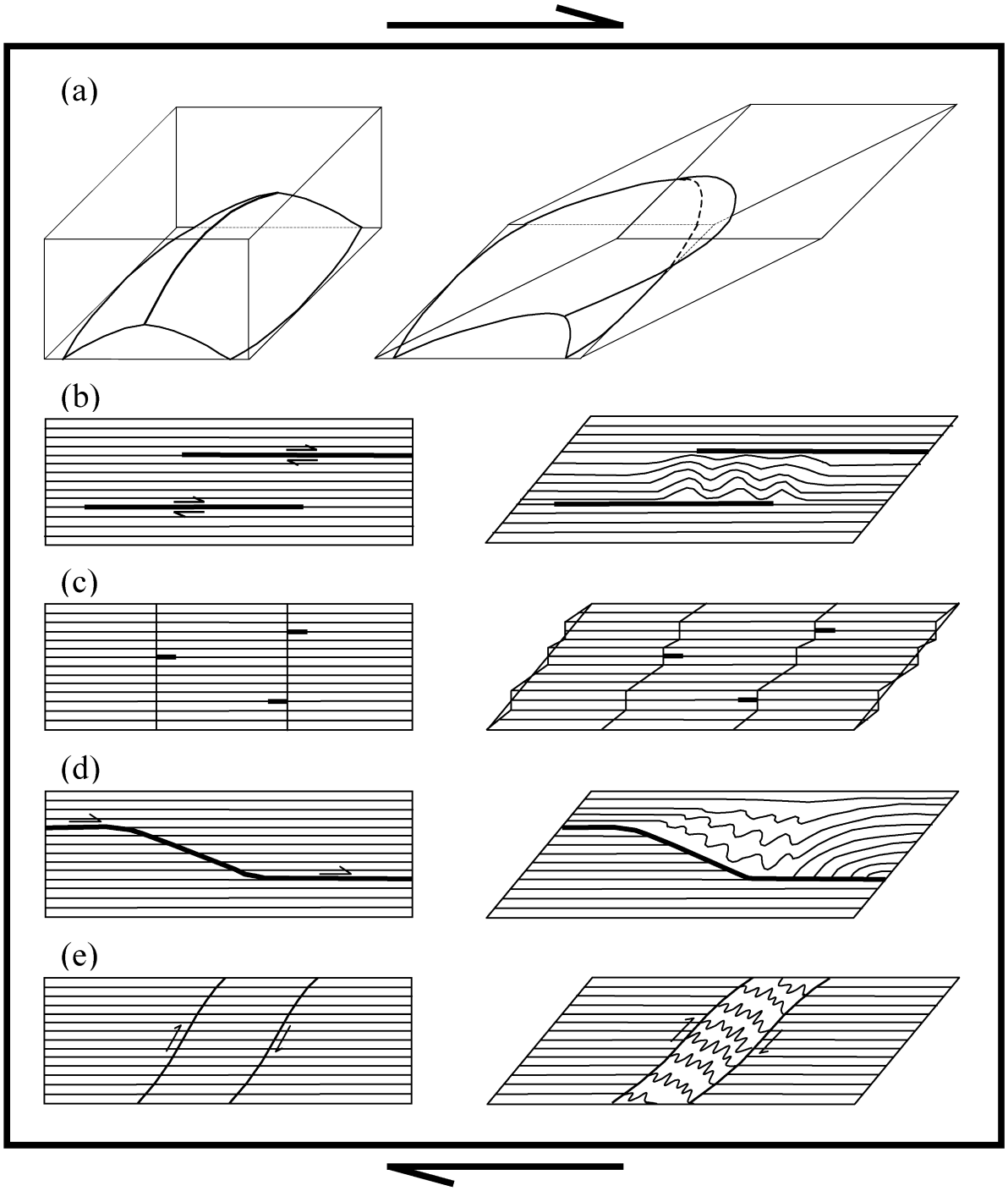

Fig. 1. Different models for the development of folds in ductile shear zones. (a) Accentuation of initial geometrical irregularities, forming strongly non-cylindrical folds (Cobbold and Quinquis, 1980; Ramsay, 1980). (b) Development of buckle folds in the contraction zone between two sidestepped slip surfaces (Passchier and Trouw, 1996). (c) Development of heterogeneous shear across the foliation due to restriction of slip at some sites (solid bar) along the foliation (Ez, 2000). (d) Folding of foliation due to curved geometry of slip surfaces (Fossen and Rykkelid, 1989). (e) Localization of folds in a segment separated by two subsidiary shear surfaces at an angle to the shear zone boundary (Ghosh and Sengupta, 1987).

field induced by rigid or stiff inclusions in ductile shear zones (Masuda and Ando, 1988; Bjornerud, 1989; Mandal et al., 2001). However, these are essentially passive folds, formed due to distortion of the foliations and cannot be compared with those we are concerned with.

This paper stems from our observations on micro-folds on the mylonitic foliation in a ductile shear zone. The development of these folds does not fit well into the available models. An alternative model is proposed to account for the development of the folds considering their

structural settings in the mylonite. The model is supported by results obtained from physical experiments and theoretical considerations.

2. Development of folds in Tangrapallium shear zone

2.1. Description of folds

Fold structures were studied in a narrow (8–10 m wide), but persistent (about half a kilometer long) shear zone within a massive granite of the Peninsular Gneissic Complex, South India (Fig. 2). The Tangrapallium shear zone is marked by foliated rocks with a nearly down-dip lineation. The angular relationship between *C*- and *S*-fabrics in mylonites indicates thrust movement in the shear zone. The angles between the two fabrics vary between 0 and 45°, as expected in simple shear deformation. Rock samples were studied in thin sections (parallel to the lineation and perpendicular to the foliation) under an optical microscope.

Micro-structural studies reveal that micro-folds occur always in close association with sericite zones that consist of extremely fine mineral grains. The zones contain specks of quartz and mica in the matrix of sericite. Chlorite often occurs in the sericite, giving a greenish tinge. Sericite zones generally occur as discrete, long lenses aligned along the *C*-fabric in mylonites (Fig. 3a). However, in places they show irregularities in their thickness and orientations, especially where the shear surfaces anastomose (Fig. 3b).

Microfolds in the mylonites occur mainly in three types of micro-structural association with sericite zones (Fig. 4). *Type A*: Thin microlithons and quartz veins, containing an internal *S*-fabric, have been folded as single layers. The internal fabric has not deformed into small folds, but is distorted in a manner that a set of parallel passive marker lines gets distorted by from a flexural slip fold. Gentle folds in lithons generally occur as symmetrical sinusoidal waves with axial planes at a high angle to the shear plane, and show a nearly class 1B (Ramsay, 1967) profile geometry (Fig. 5a). Tight folds are strongly asymmetrical and their axial planes make low angles to the shear plane (Fig. 5b). The folds and the *S* fabrics in lithons always verge in the same sense, which is consistent with the bulk shear sense. *Type B*: Closely-spaced composite microlithons generally develop single order folds (Fig. 5c; cf. Ramberg, 1968), which are of multi-order when the individual microlithons of the composite packet are interlayered with sercite zones (Fig. 5d). The lower order folds are asymmetrical, with axial planes at low angles to the shear surface, and the higher order folds that localize in the shorter limb of the lower order folds are relatively tighter and symmetrical. This polyharmonic fold geometry closely resembles those produced in buckling experiments with multilayers under layer-oblique shortening. *Type C*: Mica-rich domains, which often occur as isolated bodies, are folded in the neighborhood of sericite zones by internal kinking of the *S* fabric (Fig. 6a). The kink folds have axial planes at a high angle to the shear surface. In places, packets of microlithons, quartz veins and mica-rich layers have been folded together, where the latter two give rise to the lowest and highest order folds, respectively (Fig. 6b). Mylonites also show extensional structures locally in the form of boudins, which have developed in the microlithons.

That the folds described above developed due to buckling instabilities, is indicated by sinusoidal folds in type A, where the fold size is larger in lithons of larger thicknesses, polyharmonic folds in type B and periodic chevron folds in type C textural associations. It still remains

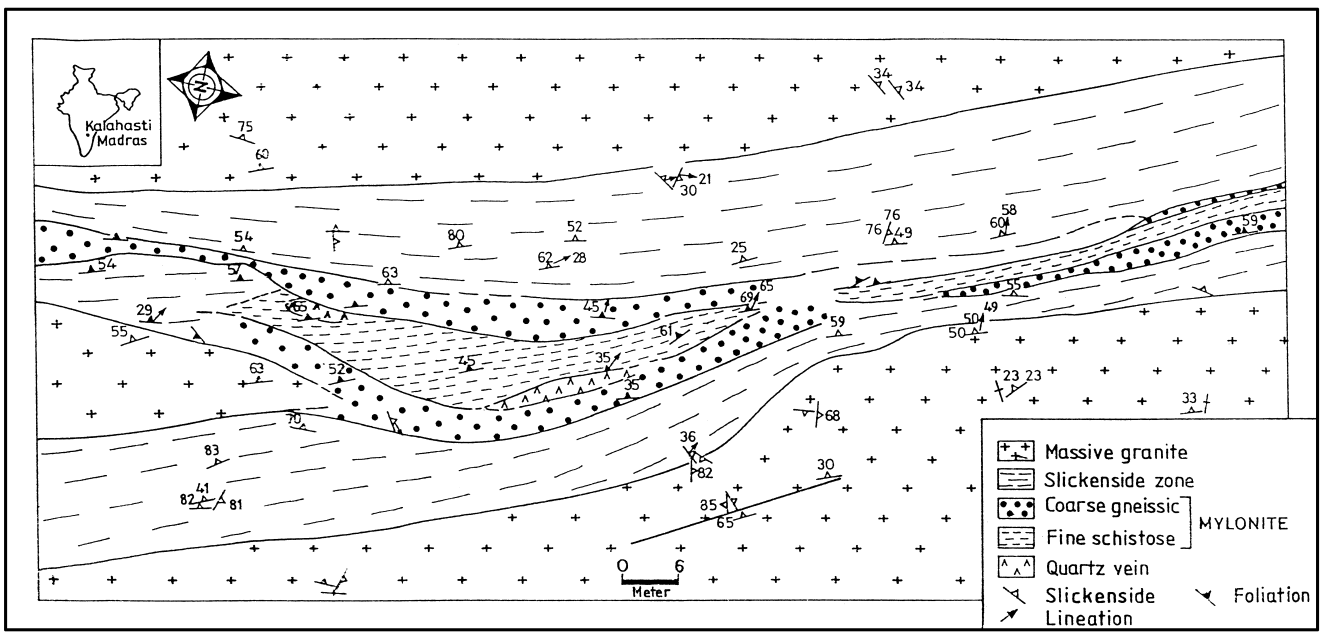

Fig. 2. Structural map of the Tangrapallium shear zone within the Peninsular Gneiss, South India.

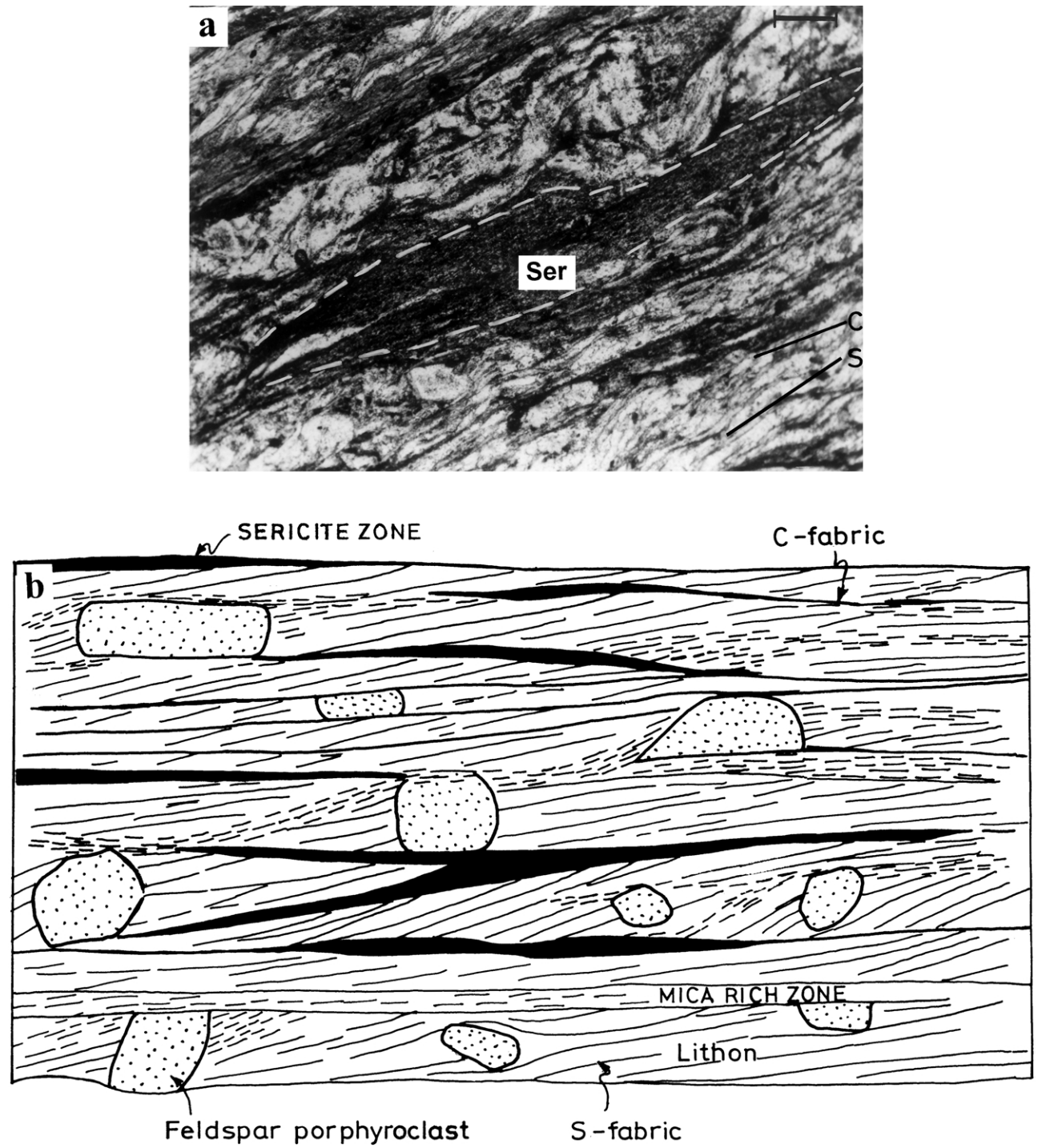

Fig. 3. (a) Lenticular sericite zone (Ser) along shear surfaces in mylonites. Scale bar: 0.25 mm. (b) Geometrical disposition of sericite (dark) zones in mylonites. (Sketch from a thin section.)

to be understood, however, how buckling is possible on *S* or *C* fabrics in the course of progressive simple shear. From the preferential localization of folds near sericite zones, we infer that the weakness of these zones relative to the surrounding medium might have induced strain heterogeneity leading to buckling instability. Based on this inference we have formulated a mechanical model for the development of buckle folds in shear zones in the course of a single, continuous deformation. The model is tested with physical experiments as well as theoretical considerations.

2.2. Weak zone model

Let us consider a shear zone characterized by homogeneously foliated rocks with a dominant *C* fabric parallel to the bulk shear plane. With progressive mylonitization,

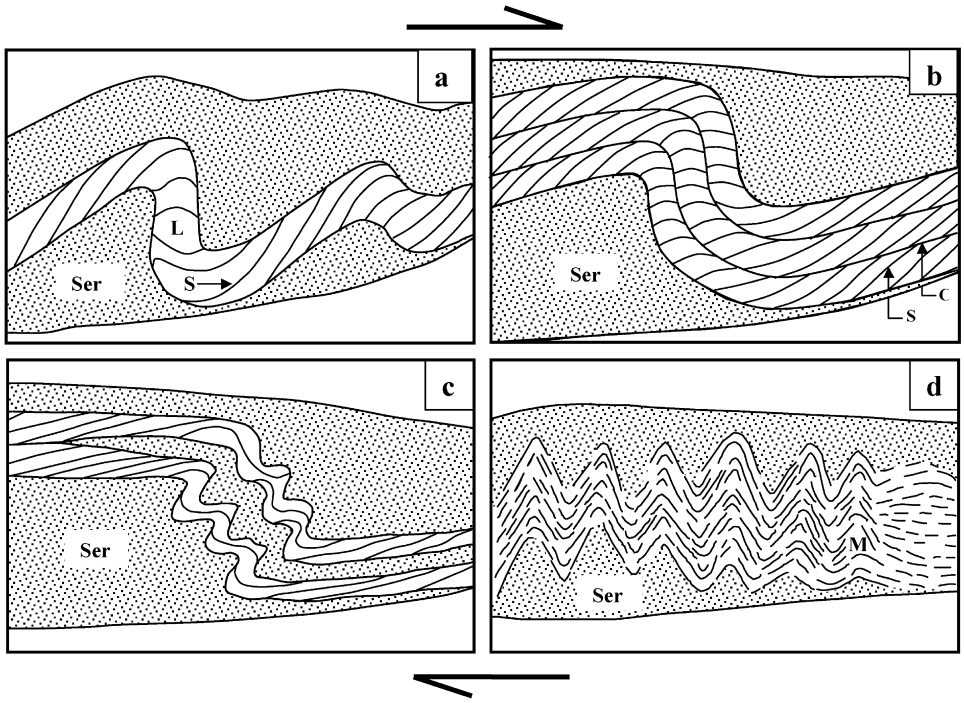

Fig. 4. Types of structural association of folds with sericite zones (Ser) in mylonites. (a) *Type A*: microlithons (L) folded as single layers while the internal *S* fabrics distorted like a set of passive markers on a flexural slip fold. (b) and (c) *Type B*: microlithons folded as composite layers harmonically and polyharmonically. (d) Type *C*: mica-rich domains (M) deformed into chevron folds.

discrete sericite zones develop along the *C* fabric, which introduce a mechanical heterogeneity resulting in local strain perturbations. The deformation in the shear zone thereby changes to be strongly heterogeneous in the course of progressive shear (Fig. 7a).

In order to understand how buckle folds nucleate in such heterogeneously deforming foliated rocks, consider a long, lenticular region in a continuous medium, filled with a material much weaker than the surrounding one (Fig. 7b), simulating a sericite zone in the mylonites. The long dimension of the weak zone is parallel to the bulk shear direction. During subsequent deformation, there will be partitioning of shear strain between the weak zone and the surrounding medium, with the weak zone accommodating larger shear strain (Treagus and Sokoutis, 1992). This strain partitioning will set up a gradient in shear along the bulk shear direction owing to a finite dimension of the weak zone. Assuming strain compatibility, the gradient in shear strain will give rise to a contraction in the bulk shear direction (Fig. 7b), which we shall show later theoretically. The contraction generated thereby can result in buckling instability on the foliation in the neighborhood of the weak zone, as revealed in physical experiments presented in the next section.

3. Experimental verification of the model

3.1. Experimental method

We ran experiments on closely spaced multilayers of plasticine. The model was about 6 cm thick, and had a length and a width of 22 and 5 cm, respectively. Two types of multilayers were used (Fig. 8). In Type 1, the multilayer simulates mylonitic microstructures with *S* fabrics nearly parallel to the *C* fabrics and Type 2: the multilayer was made analogous to typical *SC* mylonites that contain *S* fabrics oblique to the *C* fabric. In preparing the Type 1 model, 0.5-mm-thick sheets of plasticine of two contrasting colors were stacked one over another and their interfaces were smeared with grease of viscosity in the order of 10^4 Pa s. The lubrication by grease made the multilayer mechanically similar to a foliated rock. During stacking of plasticine sheets, we induced a number of thin lenticular zones of a weak material, a mixture of grease and engine oil (viscosity 24 Pa s) in a volume ratio of 4:1. Type 2 multilayers were made in a different manner. We first prepared a thick homogeneous multilayer and then cut it into a number of 3–5-mm-thick slices, at an angle of 20° with the layering. The slices were separated and stacked one over another with internal layering oblique to the model boundary. During stacking of the slices, lenticular weak zones were introduced into the multilayer. The model was then trimmed into a rectangular block.

Finally, for both types of models, the multilayer was confined by slabs of homogeneous plasticine. Two parallel vertical bars were fixed to the long faces of the model by a strong adhesive. The entire model setup was placed on a glass plate, the top surface of which was lubricated with liquid soap in order to minimize the basal friction to the model. We deformed the model under a horizontal dextral

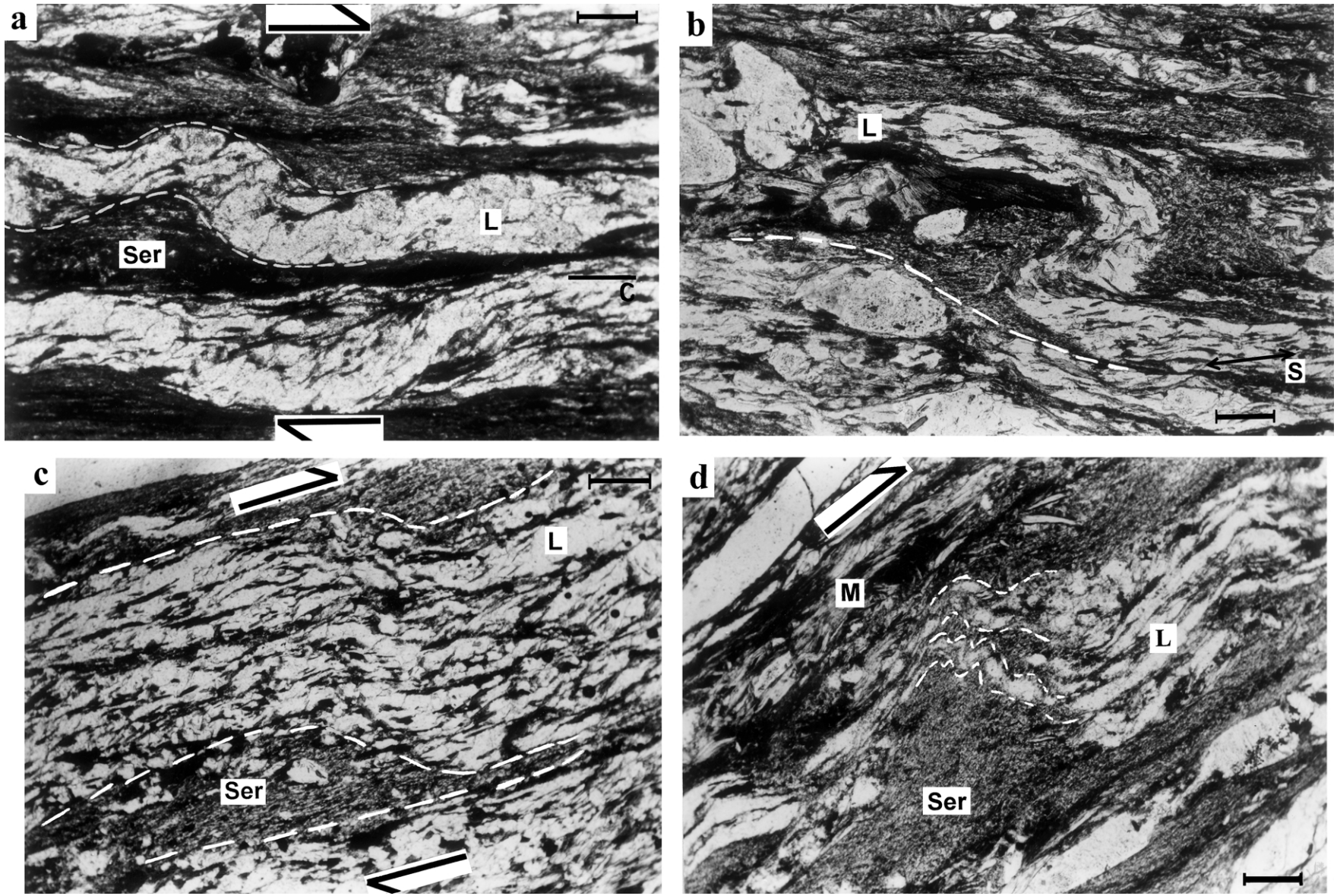

Fig. 5. Type A microfolds in mylonites: (a) nearly symmetrical folds with axial planes at a high angle to the shear surface; (b) asymmetrical folds with axial planes at low angle to the shear surface. Note that the internal *S* surfaces have been distorted like passive markers. Type B microfolds in composite lithons; (c) harmonic folds in microlithons containing closely spaced shear surfaces; (d) polyharmonic folds in microlithons with interlayered sericite zones. Note symmetrical higher order folds on the shorter limb of the larger asymmetric fold. L = microlithons; Ser = sericite zones; C = shear surfaces. Arrows indicate shear sense. Scale bar: 0.25 mm.

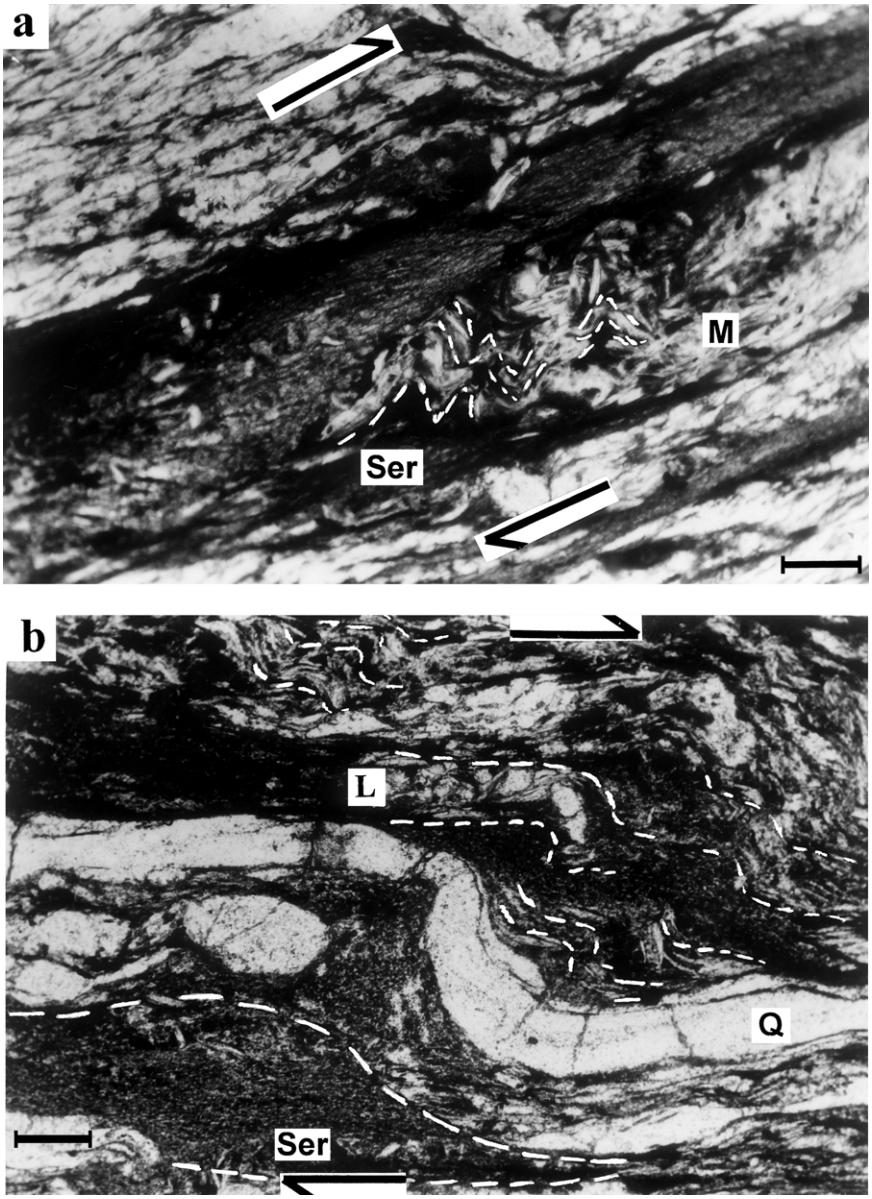

Fig. 6. (a) Chevron folds in mica-rich domains with axial planes at a high angle to the shear surface. (b) Disharmonic folds in a packet of microlithons, a quartz vein and a mica-rich domain. Ser = sericite; M = muscovite. Scale bar: 0.25 mm.

shear by moving the parallel bars in opposite directions. The progressive deformation of the model was observed and photographed from the top. After the final deformation, the sidebars were removed and the model was cut along horizontal sections at different depths to reveal the internal structures.

3.2. Experimental results

In the experiments, folds developed in the multilayer in the vicinity of the weak zones, as observed in natural mylonites. The geometry (e.g. length-to-thickness ratio) of the weak zones and their spacing across the layering or thickness of layer segment (Fig. 8) appears to be the principal factors controlling nucleation of folds. Experiments carried out by varying these two factors reveal that folds develop conspicuously when the length-to-thickness ratio of the weak zone is large and they are closely spaced separating thin layer segments. We first present results from the experiments with the Type 1 model. When the aspect ratio of weak zones was moderate (4–9) but the layer segments were thick, the multilayer deformed mainly by slip along layering, without any fold instability (Fig. 9a). However, for similar weak zones, geometry folds nucleated in the neighborhood of weak zones separating thin layer segments (Fig. 9b). The folds were initially symmetrical with their axial planes at high angles to the shear plane, but became asymmetrical, as their axial planes rotated towards the shear plane with progressive deformation. When the weak zones were very long compared with their thickness

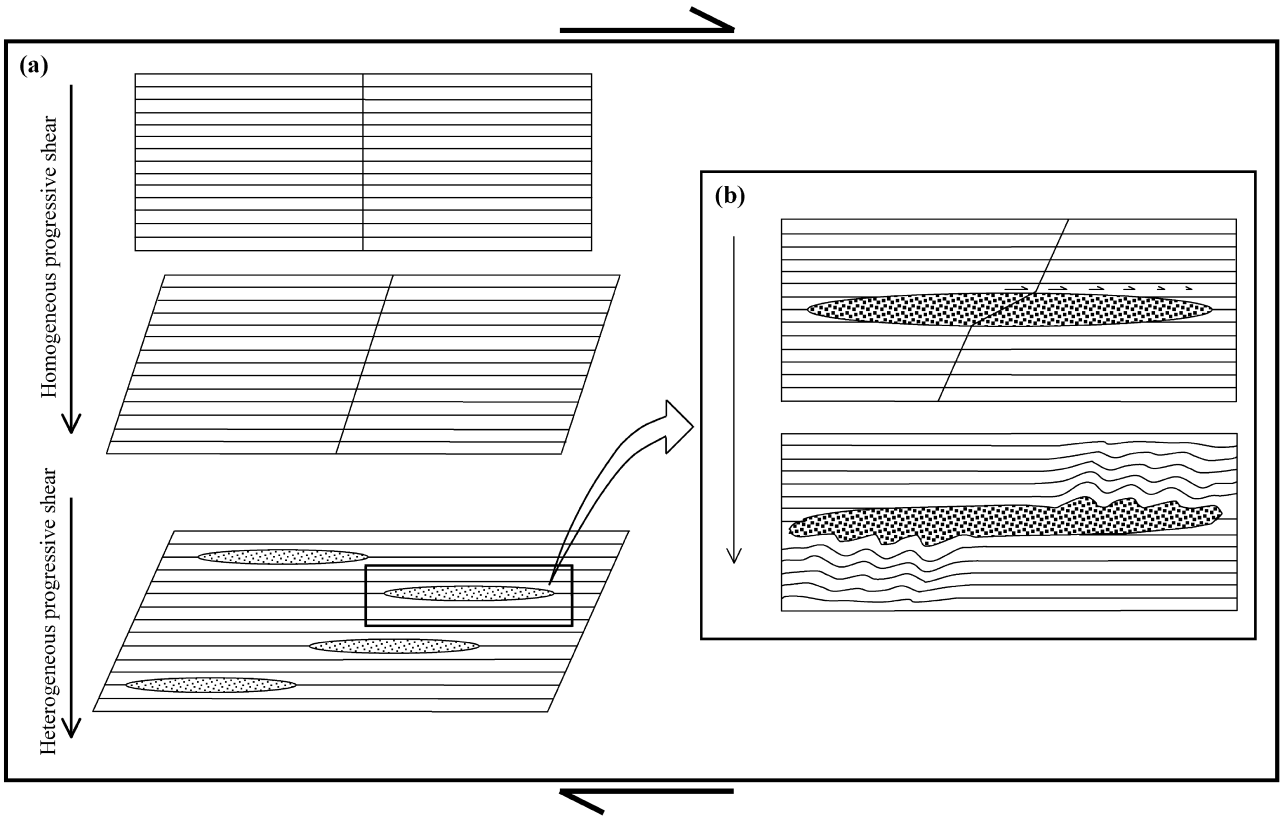

Fig. 7. Weak zone model illustrating the development of heterogeneous shear strain due to the formation of discrete sericite zones in the course of progressive deformation. Inset shows partitioning of shear strain across the foliation and its variation (shown by arrows) along the shear direction, and the onset of buckling instability on the foliation in the neighborhood of a weak zone.

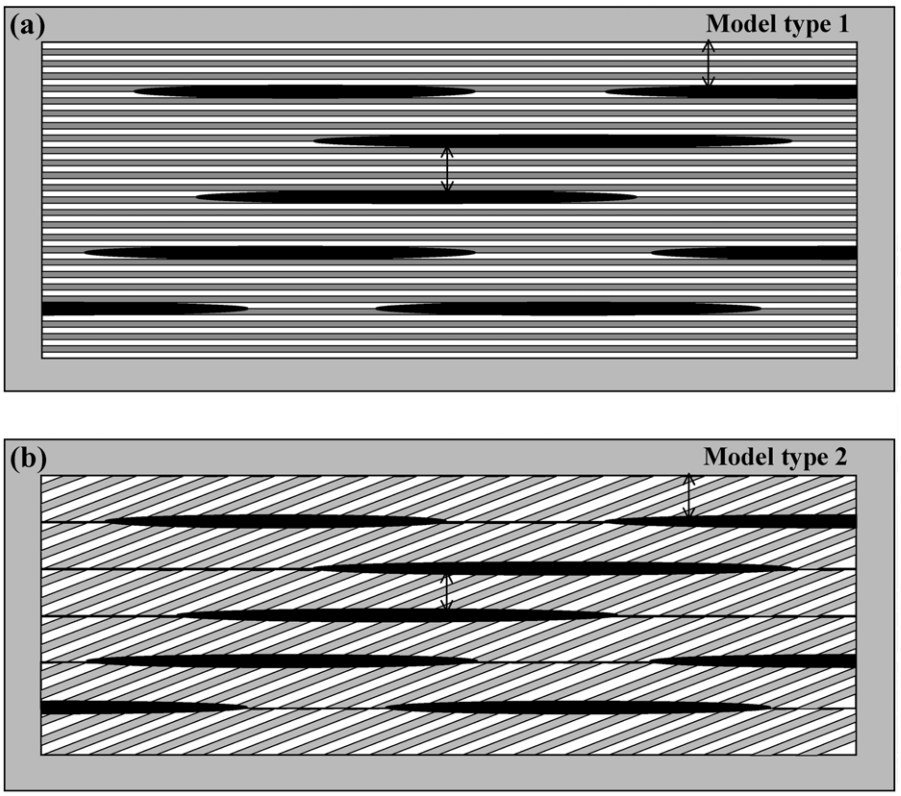

Fig. 8. Type of multilayer models used in physical experiments. (a) Type 1: multilayer simulating mylonitic microstructures with *S* fabrics nearly parallel to the *C* fabrics. (b) Type 2: multilayer simulating the microstructures of typical *SC*-mylonites. Dark-shaded areas indicate mechanically weak zones in the multilayers. Double-headed vertical arrows define layer segments considered in the analysis.

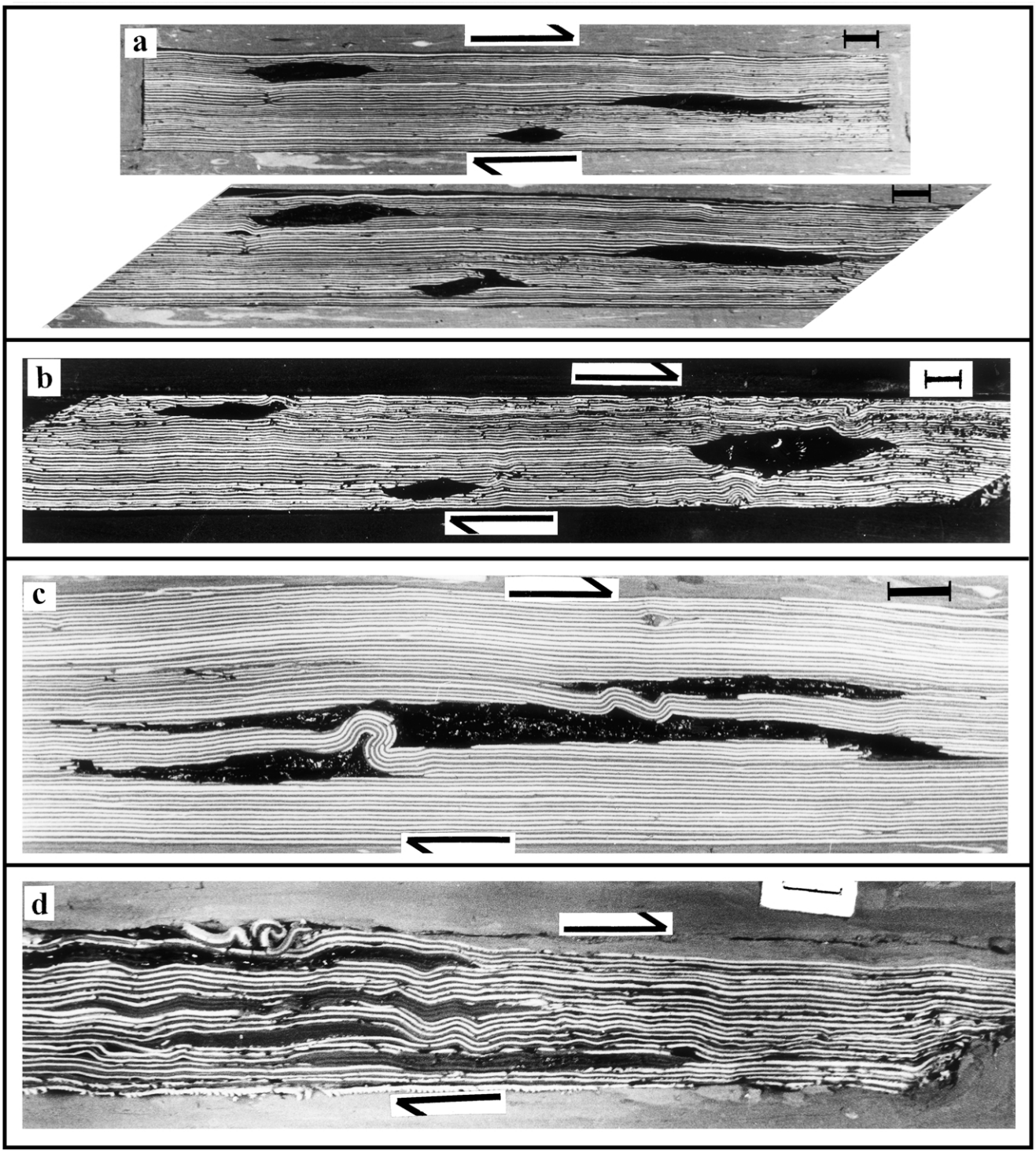

Fig. 9. Shear deformation of Type 1 model. (a) Homogeneous internal shear by layer parallel slip. Note that weak zones did not develop folds. (b) Preferential localization of folds near the tip of individual weak zones. Note that in this experiment the weak zones are isolated and non-overlapping. (c) Folds induced by weak zones with a large length-to-thickness ratio. (d) Folds of different wavelengths in multilayers containing a number of weak zones. Scale bar: 1 cm.

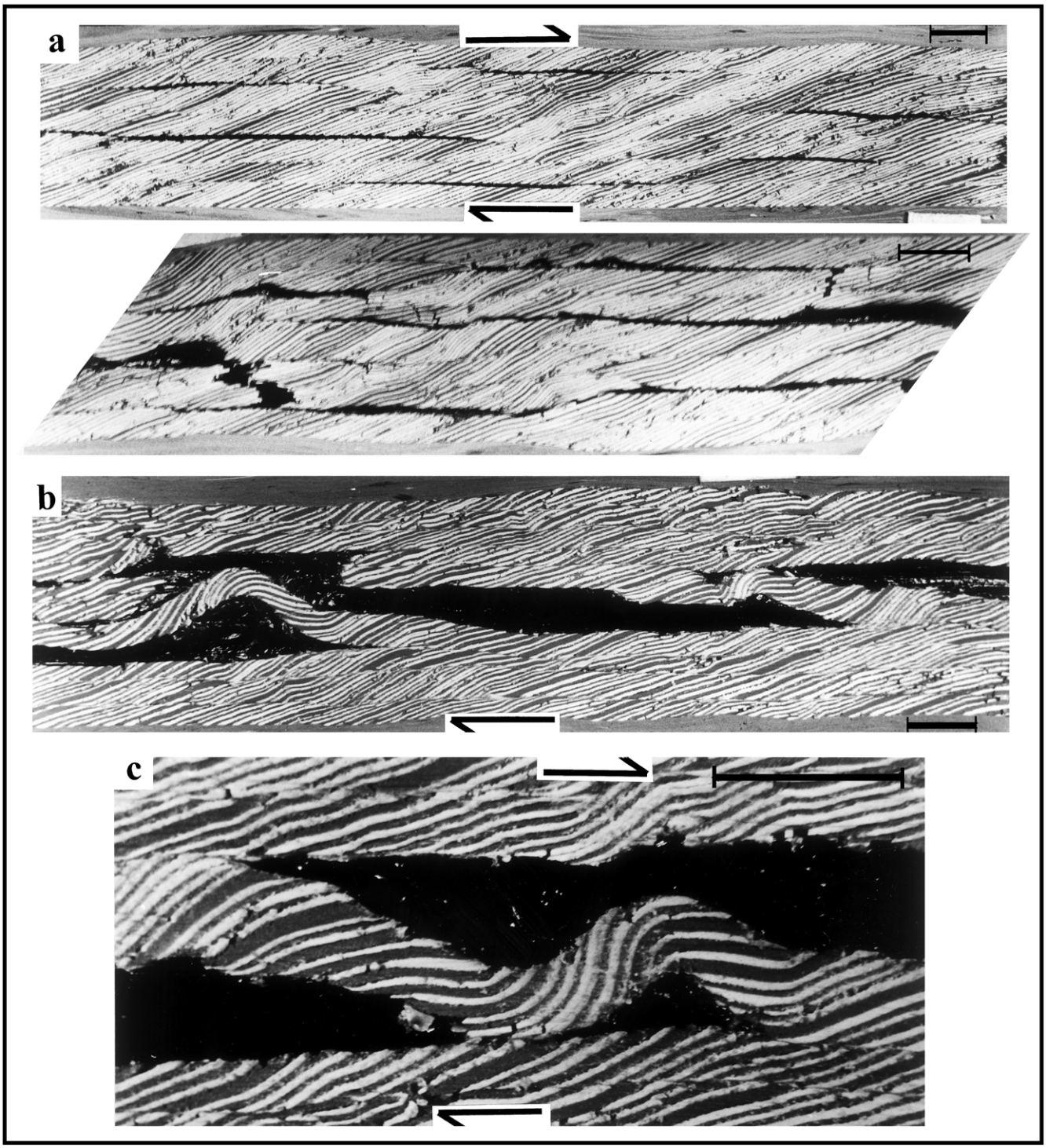

Fig. 10. Shear deformation of Type 2 model. (a) Uniform layer-parallel slip in the multilayer with weak zones, separating thick layer segments. Note that the weak zones have propagated and coalesced with one another. (b) Localization of folds in thin layer segment near weak zones with large length-to-thickness ratio. (c) Distortion pattern of internal layers by folding in a layer segment. Scale bar: 1 cm.

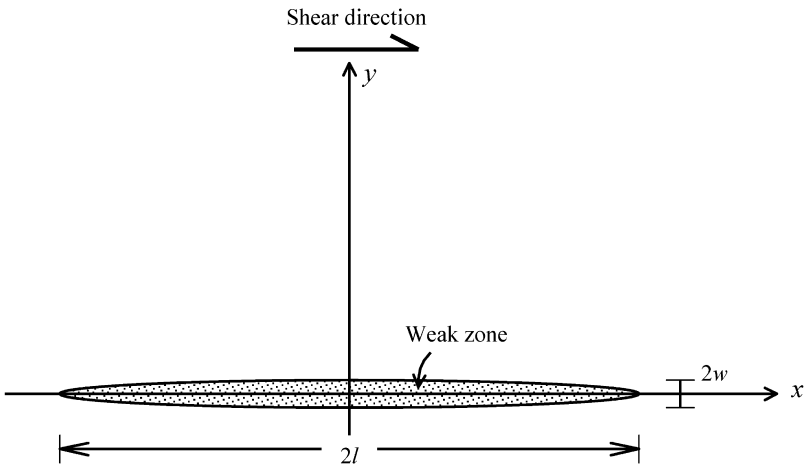

Fig. 11. Geometrical considerations in theoretical analysis.

(aspect ratio about 20), and closely spaced, spectacular folds formed in the thin layer-segments between the weak zones (Fig. 9c). The folds often developed in multiple wavelengths (Fig. 9d), as in natural mylonites (Fig. 6b).

Experiments on the Type 2 model produced similar results. Fold instability did not develop on multilayer segments when the weak zones were widely spaced. However, the presence of weak zones induced counter-rotation of the oblique fabric, resulting in steepening of the fabric near the weak zone. With a further increase in bulk shear strain, the weak zones propagated in the shear direction and coalesced with one another (Fig. 10a). Multilayers containing long (aspect ratio 20) and closely-spaced weak zones produced folds in thin layer-segments. The folds formed over a limited length of the weak zone in a single or half wave with their axial planes at right angles to the shear plane (Fig. 10b). The internal, oblique fabric did not deform into smaller folds, but were distorted like a set of passive markers on a flexural slip fold (Fig. 10c), as observed in natural in mylonites (Fig. 5a). These experiments could not be continued up to a large shear strain, but would likely have lead to development of strongly asymmetrical, folds (cf. Fig. 5b; Bons and Urai, 1996).

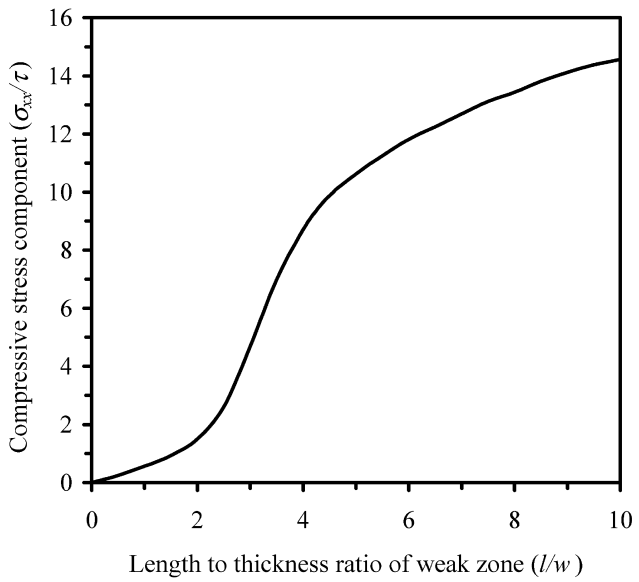

Fig. 12. Plot of compressive stress (at a point close to the tip of the weak zone) in the shear direction (σ_{xx}/τ) versus length-to-thickness ratio of the weak zone (l/w). τ: far-field shear stress.

It is evident from the experimental findings that under certain circumstances, buckling instability may develop even in progressive simple shear on the mylonitic foliation due to the presence of weak zones, as conceived in our *Weak Zone Model*. In the following section, we present a theoretical analysis to show how such weak zones perturb the stress field and may, depending on their geometry, develop compressive stresses parallel to the shear direction, thereby triggering a buckling instability.

4. Theoretical analysis

Consider an elliptical weak zone of length, $2l$, and thickness, $2w$, in a two-dimensional space, representing the plane normal to the shear zone and along the shear direction. A Cartesian reference frame xy is chosen at the center of the weak zone with the x-axis along the long axis of the weak zone, which is oriented parallel to the bulk shear direction (Fig. 11). In this analysis we employ the complex variable method in which a two-dimensional space (x, y) can be expressed in terms of a single mathematical parameter z, where $z = x + iy$. The plane containing the weak zone is designated as the z plane in the following discussion. According to the theory of plane stress (Muskhelishvilli, 1953), the stress field outside the weak zone can be expressed as:

$$\sigma_{xx} + \sigma_{yy} = [\varphi'(z) + \overline{\varphi'(z)}] \quad (1a)$$

$$\sigma_{yy} - \sigma_{xx} + 2\sigma_{xy} = 2[\bar{z}\varphi''(z) + \psi'(z)] \tag{1b}$$

where $\varphi(z)$ and $\psi(z)$ are complex functions. Single and double primes indicate their first and second derivatives with respect to z, and bars represent conjugates of the complex functions. The z-plane is subjected to a far-field shear stress, τ, in the x direction. We assume that the material inside the weak zone is much weaker than the material occurring outside the weak zone and thereby its traction on the boundary of the weak zone is considered to be negligibly small. It can be shown that under this condition the functions $\varphi(z)$ and $\psi(z)$ have the following expressions:

$$\varphi(z) = \frac{2i\tau R^2}{z+N} \tag{2}$$

$$\psi(z) = \frac{i\tau R}{2}\left[(z+N) + \frac{4R^2}{m}\left\{\frac{m^2+1}{2N} - \frac{1}{z+N}\right\}\right] \tag{3}$$

where

$$N = \sqrt{z^2 - 4mR^2}$$

$$m = \frac{l-w}{l+w}$$

$$R = \frac{l+w}{2}$$

Differentiating Eqs. (2) and (3) with respect to z, and substituting their expressions in Eqs. (1a) and (1b), we have:

$$\sigma_{xx} + \sigma_{yy} = 8\tau R^2 L \tag{4}$$

$$\sigma_{yy} - \sigma_{xx} + 2i\sigma_{xy} = 2\tau R[(H + iJ) - R(G - iF)] \tag{5}$$

After separating the real and the imaginary parts of Eq. (5), we get:

$$\sigma_{yy} - \sigma_{xx} = -2\tau R(2GR - H) \tag{6a}$$

$$\sigma_{xy} = \tau R[2RF + J] \tag{6b}$$

The expressions of the parameters in the above equations are:

$$a = x^2 - y^2 - 4mR^2$$

$$b = 2xy$$

$$c = \pm\left[\frac{1}{2}\left\{\left(a^2+b^2\right)^{\frac{1}{2}} + a\right\}\right]^{\frac{1}{2}}$$

$$d = \pm\left[\frac{1}{2}\left\{\left(a^2+b^2\right)^{\frac{1}{2}} - a\right\}\right]^{\frac{1}{2}}$$

$$A = \frac{xc + yd}{c^2 + d^2}$$

$$B = \frac{yc - xd}{c^2 + d^2}$$

$$K = \frac{(xc - yd + a)}{(xc - yd + a)^2 + (xd + yc + b)^2}$$

$$L = -\frac{(xd + yc + b)}{(xc - yd + a)^2 + (xd + yc + b)^2}$$

$$E = \frac{x(c^3 - 3cd^2) - y(d^3 - 3c^2 d)}{(c^2 + d^2)^3}$$

$$F = \frac{x(c^3 - 3cd^2) + y(d^3 - 3c^2 d)}{(c^2 + d^2)^3}$$

$$Q = \frac{x(d^3 - 3c^2 d) + y(c^3 - 3cd^2)}{(c^2 + d^2)^3}$$

$$G = \frac{x(d^3 - 3c^2 d) - y(c^3 - 3cd^2)}{(c^2 + d^2)^3}$$

$$J = \frac{1+A}{2R} + \frac{4R^2}{m}K - 2R^2\frac{(m^2+1)}{m}E$$

$$H = B + \frac{4R^2}{m}L - 2R\frac{m^2+1}{m}Q$$

The stress components, σ_{xx}, σ_{yy} and σ_{xy} at any point (x, y) in the neighborhood of the weak zone can now be determined from Eqs. (4), (6a) and (6b). For the present problem we made a numerical analysis for the compressive stress component, σ_{xx}, and the orientations of the principal

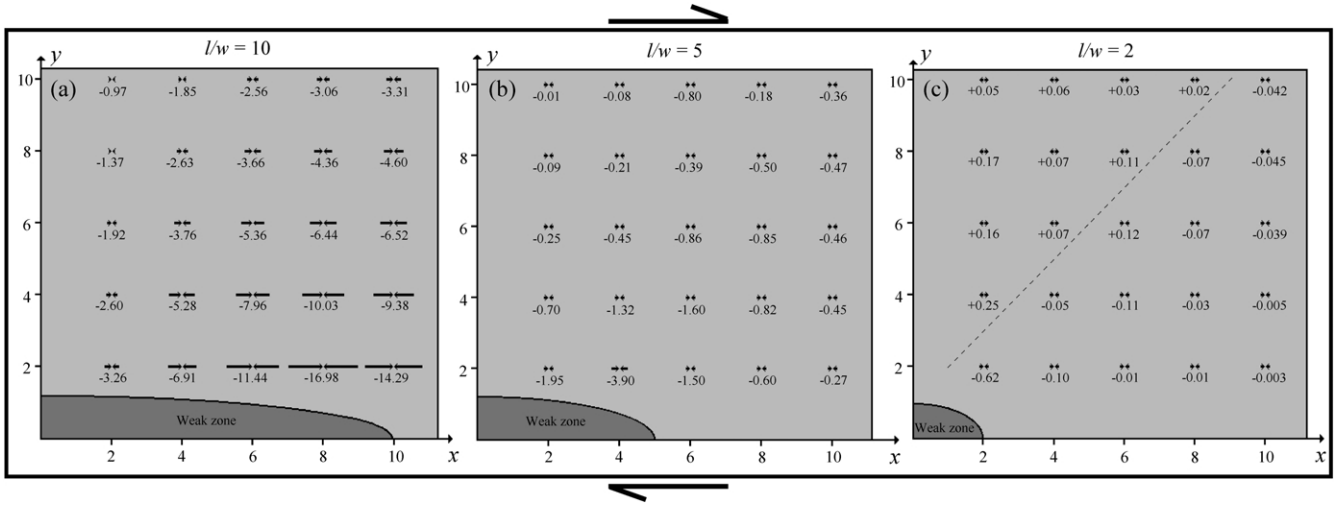

Fig. 13. Variations in the magnitude of local compressive stresses parallel to the shear direction in numerical models containing weak zones of different aspect ratios (l/w). The magnitude is normalized to the far-field shear stress (σ_{xx}/τ).

axes of stress:

$$\tan(2\alpha) = \frac{2\sigma_{xy}}{\sigma_{xx} - \sigma_{yy}} \quad (7)$$

where α is the inclination of the principal axes of stress to the bulk shear direction.

With the help of a simple computer programme in BASIC for Eqs. (4)–(7), we numerically analyzed the stress distribution in the positive quadrant of z space under a dextral far-field shear stress, τ. The compressive stress component, σ_{xx}, near the tip of a weak zone increases steeply with increasing length-to-thickness ratio (l/w) of the weak zone (Fig. 12). Numerical simulations were run for $l/w = 2$, 5 and 10 to reveal the control of weak zone geometry on the stress distribution. When $l/w = 10$, compressive stresses develop in the bulk shear direction over a large extent, showing a maximum at a point close to the tip of the weak zone (Fig. 13a). The magnitude of compressive stress decreases away from the weak zone. Numerical models with $l/w = 5$ also show localization of shear-parallel compressive stresses near the weak zone (Fig. 13b). However, the intensity of the stress concentration (measured in terms of spatial extent as well as magnitude) is weaker than that in the earlier model. The weak zone develops virtually no compressive stress along the bulk shear direction, when $l/w = 2$ (Fig. 13c).

Using Eq. (7), we map the trajectory of the principal compression axis in the neighborhood of a weak zone. Models with $l/w = 2$ and 5 do not show a significant heterogeneity in the orientation distribution (Fig. 14a and b). Except very near to the weak zone, the principal axes are oriented at an angle of 45° to the bulk shear direction, as expected in an ideal shear zone. But, when $l/w = 10$, the orientation distribution is strongly heterogeneous near the weak zone, showing a large area where the principal axis of compression is oriented at a low angle to the bulk shear

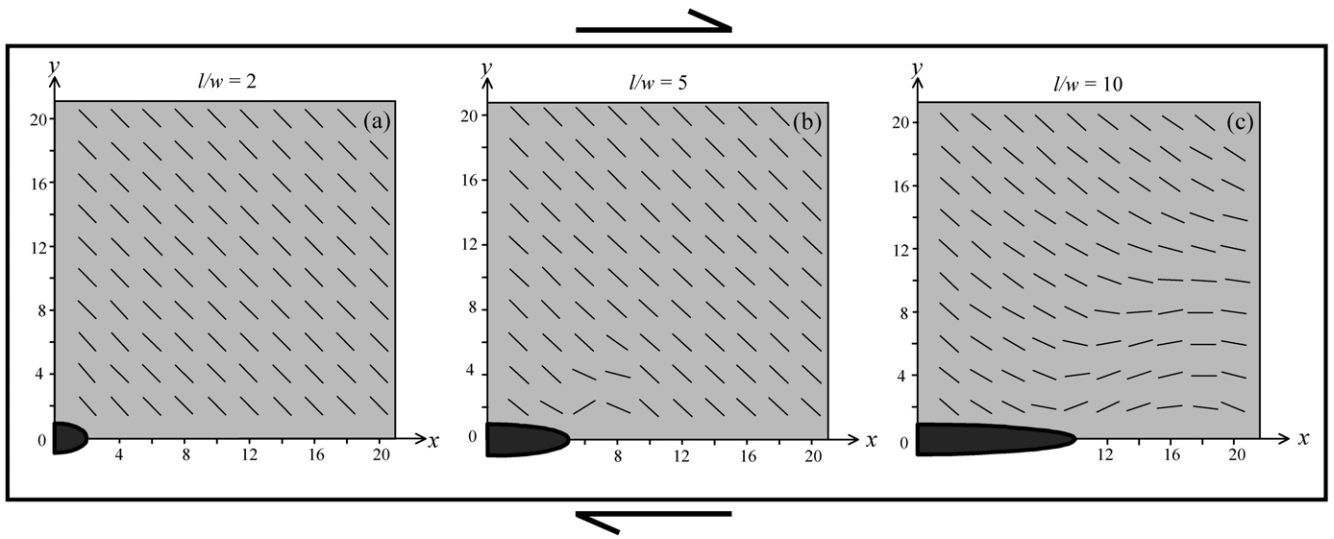

Fig. 14. Trajectories of the principal axis of compressive stress in the neighborhood of weak zones of different aspect ratios (l/w) in numerical models.

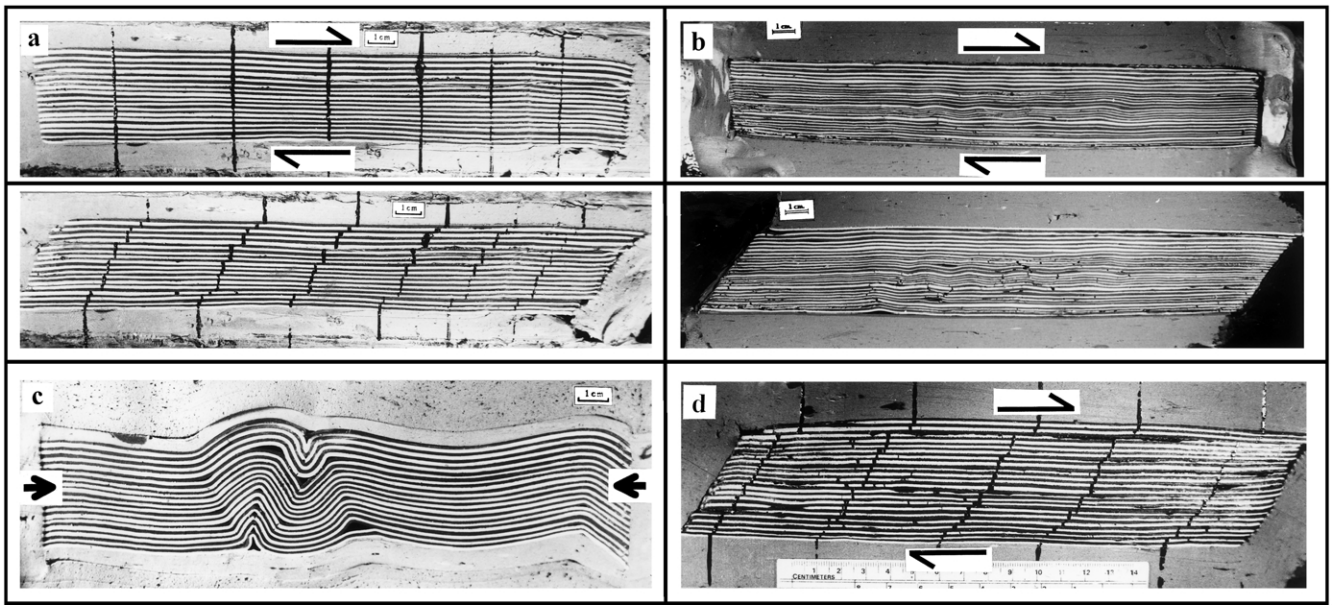

Fig. 15. (a) Heterogeneous shear deformation in a multilayer model. The layer interfaces were non-uniformly lubricated with oil to simulate heterogeneous slip along layering. (b) Deformation of multilayer model containing incipient geometrical irregularities in the form of sinusoidal waves (center). Note that the geometrical waves did not amplify in the course of foliation-parallel shear. (c) and (d) Deformation of mechanically homogeneous anisotropic multilayer under layer-parallel compression and shear, respectively. Note that buckling instability did not develop under layer-parallel shear, even when the degree of anisotrophy is strong, favoring buckling instability under layer-parallel shortening.

direction, and is locally inclined in the opposite direction (Fig. 14c). In summary, the numerical simulations indicate: (1) the degree of perturbation in the shear stress field will be larger for a larger length-to-thickness ratio of weak zone; and (2) a weak zone can develop local contraction in the shear and even in the bulk extension direction.

5. Discussion

Ductile shear zones generally record folding on the mylonitic foliation. However, it is not clearly understood how schistosities that develop parallel to the *XY* plane of strain or along the shear direction can be shortened and folded in the same deformation, unless we assume the deformation to be of pulsating type. Based on micro-scale observations in natural mylonites, the model presented in this paper needs to be reviewed in the light of previous models or hypotheses, considering three physical factors: (1) heterogeneous slip, (2) initial geometrical irregularity, and (3) degree of mechanical anisotropy.

It has been suggested that shortening can develop locally along the schistosity due to heterogeneous slip, which may lead to folding on the schistosity (Ghosh and Sengupta, 1987). We verified this proposition by performing physical experiments on multilayer models consisting of very thin layers (0.5 mm). The interfaces of layers were non-uniformly lubricated with oil in order to simulate heterogeneous slip in the layered system. The models were deformed under layer parallel simple shear. But none of the experiments produced folds on the layers (Fig. 15a). The heterogeneous slip hypothesis thus seems inappropriate in explaining the formation of folds in the Tangrapallium shear zone.

We also tested whether initial geometrical irregularities could grow and give rise to fold structures (cf. Cobbold and Quinquis, 1980; Ramsay, 1980). For this, incipient waves of low amplitude were induced in the initial model. Under layer-parallel shear the waves did not grow in amplitude (Fig. 15b).

Mechanical anisotropy and heterogeneity (i.e. lensoid nature of the weak spots) apparently seems to be a controlling factor in triggering folds in ductile shear zones. In the Tangrapallium shear zones, homogeneous, massive granite has been progressively transformed into a foliated (mechanically anisotropic) rock. It may appear that synkinematic sericitization has enhanced the degree of anisotropy in mylonites, causing nucleation of fold structures. However, the degree of mechanical anisotropy is a necessary, but not sufficient, factor in triggering fold instability under consideration. In order to confirm this, we carried out a few experiments on homogeneously foliated models. The models developed folds rapidly under a slight amount of shortening parallel to the foliation (Fig. 15c), but they never showed such instability under foliation parallel shear. The model deformed homogeneously involving uniform glides of layers one over another (Fig. 15d). The experimental results rule out the possibility of mechanical anisotropy as a triggering factor for folding in ductile shear zones.

It is evident that the formation of micro-folds in the Tangrapallium shear zone cannot be readily explained by

any of the existing hypotheses. We therefore propose an alternative *Weak Zone Model*, which is also based on mechanical heterogeneity. However, in contrast to earlier ones, our model indicates that the heterogeneity must be in the form of discrete bodies containing materials much weaker than the surrounding material. It may be noted that buckling of a layer or any segment of rock mass will involve deformation of the surrounding material, which has to be sufficiently weak. Thus, the material within the weak zone flows easily as the stiff layer segments buckle, as in case of décollement folding. In case of a system where mechanical heterogeneity is induced by discrete slip surfaces, buckling would require a large stress in order to strain the surrounding stiff system. The simple model experiments show that it is difficult for a slip surface to induce folds in its neighborhood (Fig. 15a). In such a system, either of two processes can operate: (1) layer-parallel shear would be heterogeneously distributed across the layering, as suggested by Ez (2000), or (2) the slip surfaces could propagate along its length of the system, releasing the contraction along the shear direction.

6. Conclusions

1. In the Trangapallium ductile shear zone, micro-folds have developed by buckling of the mylonitic foliation in response to local contraction parallel to the bulk shear direction.
2. Folding in the shear zone is difficult to explain using any of several existing models, involving heterogeneous slip along foliation; accentuation of geometrical irregularity with progressive shear; curvilinear shear surfaces and mechanical anisotropy in the foliated rocks, which are, however, applicable in other settings.
3. This new model demonstrates that discrete mechanically weak zones, developed because of synkinematic sericitization, perturb the homogeneous shear stress field, developing a local compressive stress component along the foliation, which subsequently lead to buckling instability on the foliation.
4. The flow of material in the weak zones is required in the development of folds in the stiffer unit in its neighborhood.
5. The length-to-thickness ratio of weak zones is a crucial parameter determining the magnitude of local compressive stresses developed along the bulk shear direction.

Acknowledgements

We thank Professors P. Bons and M. Bjornerud for their critical comments and Professor R.J. Norris for giving an outline in revising the manuscript. We are grateful to Dr S. Hanmer for his valuable remarks on an early version of the manuscript. This work was supported by the DST, India. CC acknowledges infrastructural facilities provided by the Indian Statistical Institute, Calcutta.

References

Bjornerud, M., 1989. Mathematical model for folding of layering near rigid objects in shear deformation. Journal of Structural Geology 11, 245–254.

Bons, P.D., Urai, J.L., 1996. An apparatus to experimentally model the dynamics of ductile shear zones. Tectonophysics 256, 145–164.

Cobbold, P.R., Quinquis, H., 1980. Development of sheath folds in shear regimes. Journal of Structural Geology 2, 119–126.

Ez, V., 2000. When shearing is a cause of folding. Earth-Science Reviews 51, 155–172.

Fossen, H., Rykkelid, E., 1989. Shear zone structures in the Oygarden area, West Norway. Tectonophysics 174, 385–397.

Ghosh, S.K., Sengupta, S., 1987. Progressive evolution of structures in a ductile shear zone. Journal of Structural Geology 9, 277–288.

Harris, L.B., 2003. Folding in high-grade rocks due to back-rotation between shear zones. Journal of Structural Geology 25, 223–240.

Honge, F.D., Hippertt, J.F., 2001. Quartz crystallographic and morphologic fabrics during folding/transposition in mylonites. Journal of Structural Geology 23, 81–92.

Mandal, N., Samanta, S.K., Chakraborty, C., 2001. Numerical modeling of heterogeneous flow fields around rigid objects with special reference to particle paths, strain shadows and foliation drag. Tectonophysics 330, 177–194.

Masuda, T., Ando, S., 1988. Viscous flow around a rigid spherical body: a hydrodynamical approach. Tectonophysics 148, 337–346.

Mawer, C.K., Williams, P.F., 1991. Progressive folding and foliation development in a sheared, coticule-bearing phyllite. Journal of Structural Geology 13, 539–555.

Muskhelishvilli, N.I., 1953. Some Basic Problems of Mathematical Theory of Elasticity, Noordhoff, Groningen, 704pp.

Passchier, C.W., Trouw, R.A.J., 1996. Microtectonics, Springer, Germany.

Ramberg, H., 1968. Instability of layered systems in the field of gravity, I, II. Physics Earth Planetary Interiors 1, 427–447.

Ramsay, J.G., 1967. Folding and Fracturing of Rocks, McGraw-Hill, New York, 568pp.

Ramsay, J.G., 1980. Shear zone geometry: a review. Journal of Structural Geology 2, 83–99.

Treagus, S.H., Sokoutis, D., 1992. Laboratory modelling of strain variation across rheological boundaries. Journal of Structural Geology 14, 405–424.